HHS Public Access

Author manuscript

Proc SPIE Int Soc Opt Eng. Author manuscript; available in PMC 2017 August 25.

Published in final edited form as:

Proc SPIE Int Soc Opt Eng. 2017 February ; 10133: . doi:10.1117/12.2254545.

Effects of b-Value and Number of Gradient Directions on Diffusion MRI Measures Obtained with Q-ball Imaging

Kurt G. Schilling[a], **Vishwesh Nath**[b], **Justin Blaber**[c], **Robert L. Harrigan**[a,c], **Zhaohua Ding**[a], **Adam W Anderson**[a], and **Bennett A Landman**[a,b,c]

[a]Vanderbilt University Institute of Imaging Science, Vanderbilt University, Nashville, TN

[b]Computer Science, Vanderbilt University, Nashville, TN

[c]Electrical Engineering, Vanderbilt University, Nashville, TN

Abstract

High-angular-resolution diffusion-weighted imaging (HARDI) MRI acquisitions have become common for use with higher order models of diffusion. Despite successes in resolving complex fiber configurations and probing microstructural properties of brain tissue, there is no common consensus on the optimal b-value and number of diffusion directions to use for these HARDI methods. While this question has been addressed by analysis of the diffusion-weighted signal directly, it is unclear how this translates to the information and metrics derived from the HARDI models themselves. Using a high angular resolution data set acquired at a range of b-values, and repeated 11 times on a single subject, we study how the b-value and number of diffusion directions impacts the reproducibility and precision of metrics derived from Q-ball imaging, a popular HARDI technique. We find that Q-ball metrics associated with tissue microstructure and white matter fiber orientation are sensitive to both the number of diffusion directions and the spherical harmonic representation of the Q-ball, and often are biased when under sampled. These results can advise researchers on appropriate acquisition and processing schemes, particularly when it comes to optimizing the number of diffusion directions needed for metrics derived from Q-ball imaging.

Keywords

Diffusion; Q-ball; Reproducibility; HARDI; Gradient Directions; b-value

1. INTRODUCTION

Diffusion tensor imaging (DTI) is arguably the most commonly used diffusion-weighted magnetic resonance imaging (dMRI) technique due to its simplicity and its ability to provide unique insights into tissue microstructure {Basser, 1994 #2}. These insights include metrics that have been associated with white matter integrity as well as estimates of dominant white matter directions, which enable fiber tractography {Mori, 2002 #9}. However, DTI only models a single diffusion direction per voxel, and is inadequate in areas that contain multiple fiber populations, often resulting in incorrect estimates of fiber orientation or misleading

Correspondence to: Kurt G. Schilling.

microstructural indices. The “crossing fiber” problem has been shown to be prevalent in dMRI datasets, affecting as much as 90% of all voxels in the brain {Jeurissen, 2013 #330}. To address this issue, a variety of higher order diffusion models have been introduced. These methods are generally referred to as high-angular-resolution diffusion-weighted imaging (HARDI), a term which encompasses nearly all acquisition and analysis pipelines that provide more information than the diffusion tensor – but most commonly indicating the acquisition of a large number of diffusion weighted images (DWIs) sensitized to diffusion along varying directions all acquired at the same b-value, or diffusion weighting (DW).

Despite the rapidly growing popularity of HARDI techniques, there is currently no fixed consensus on the optimal b-value for these methods, or on the appropriate number of diffusion directions for these methods. Early DTI studies addressed the optimal b-value and diffusion direction schemes by acquiring multiple repeats of unique acquisition schemes, and assessed the impact on the precision and accuracy of orientation estimates and microstructural indices {Landman, 2007 #75}. However, similar studies have not been performed on HARDI models, in part due to the tremendous acquisition requirements needed for this type of analysis. Thus, most knowledge of appropriate acquisition requirements comes from simulations and phantom data {Jansons, 2003 #3}.

Rather than analyze a specific HARDI model, Tournier et al. have addressed this question of sampling directions by analyzing the frequency content of the DW signal itself, fit to spherical harmonics (SH) {Tournier, 2013 #1}. They concluded that the angular profile of the DW signal at a b-value of 1000 s/mm^2 could be captured with order 4 SH, requiring only 15 unique sampling directions. Similarly, b-values up to 3000 s/mm^2 require only 28 unique directions (6 SH) to capture the necessary information. However, these numbers represent lower bounds, much like the diffusion tensor only requires 6 measurements, but in practice up to 30 are typically acquired. Thus, it remains to be seen how many sampling directions, and what b-value, are needed for HARDI models in practice.

In this study, we focus on one common HARDI model called Q-Ball imaging, or just Q-ball {Tuch, 2004 #4}. By acquiring 11 repeats of a high-angular-resolution dataset, we probe the precision and accuracy of estimating various Q-ball metrics as a function the number of sampling directions. Specifically, we use Q-ball to derive the diffusion orientation distribution function (dODF), from which we derived reproducibility measures of fractional anisotropy (FA), generalized fractional anisotropy (GFA). We then extract peaks of the dODF in order to assess the reproducibility of the orientations and strengths of the peaks, the Hessian of each peak (which describes its curvature), as well as the number of detected fiber populations (or peaks) in each voxel. Finally, we assess the angular correlation coefficient (ACC) of the dODFs between each individual dataset and the dataset acquired with the full complement of diffusion directions.

2. METHODS

2.1 MRI acquisition

All imaging was performed on the same healthy volunteer scanned on a 3T Phillips Achieva Scanner (Philips Medical Systems, Best, The Netherlands), in three different two-hour long

sessions, on three consecutive days. The scanning protocol consisted of five diffusion shells (b-values of 1000, 1500, 2000, 2500, and 3000 s/mm^2) with 96 diffusion-weighted directions each, plus five repeats of the non-DW (b0) volume, which were formed by 10 scanner averages. The data was acquired at 2.5mm isotropic resolution, with a matrix of 96 × 96 × 38 slices, using a DW PGSE-EPI sequence. Briefly, scan parameters were: Multi-Band=2; SENSE=2.2; TR= 2650 ms; TE=94 ms; Partial Fourier=0.7. Fold over direction was A-P with a P fat shift. For each set of 5 shells, an additional "b0" was acquired with reverse phase encoded volumes (i.e., fold over direction A-P with A fat shift). This protocol was repeated four times on days 1 and 2, and three times on day 3, resulting in a total of 11 repeats of each diffusion shell.

2.2 Q-ball processing

All volumes were corrected for movement, susceptibility induced distortions, and eddy currents using FSL's topup and eddy {Andersson, 2003 #13;Andersson, 2016 #14}. All data was registered to a common space using a 6 degrees-of-freedom rigid registration to facilitate a voxel-wise comparison, followed by appropriate re-orientation of diffusion gradient vectors. The full 96 gradient directions were re-ordered to minimize the electrostatic potential of any partial set of the first "N" directions, ensuring that the first "N" directions are as maximally uniformly distributed. From this, for each diffusion shell, subsets of DWIs from 20 to 96 directions (in increments of 4) were created and analyzed with the Q-ball model using UCL's Camino Diffusion MRI Toolkit {Cook, 2006 #6}. This results in an approximation of the dODF (represented using SH coefficients), from which various microstructural and fiber orientation metrics are derived. It is important to note that the Q-ball is derived using the highest order SH coefficients possible (up to order 8) given the number of sampling points (i.e. < 28 directions = SH order 4; 28–44 directions = SH order 6; > 44 directions = SH order 8).

2.3 Metrics and analysis

For every diffusion shell (11 repeats of each of 5 b-values), and all subsets of directions within each shell, various metrics were derived, and compared directly to the corresponding full 96-direction dataset as a gold standard. First, FA was calculated using the DTI model, while GFA was calculated directly from the Q-ball SH coefficients. Next, local maxima, or peaks, in the dODF were detected following Jansons and Alexander {Jansons, 2003 #3}. From each peak, one can first determine its curvature (or sharpness) using the trace of the hessian. Because each peak is traditionally assumed to represent a distinct population of fiber bundles, the fiber fraction of each peak can be calculated (in this study DFF represents the dominant fiber fraction) and the number of fiber bundles (peaks) per voxel. The ability of each subset to detect crossing fiber voxels can be described by the consistency fraction (CF). A voxel is consistent with the gold standard if it has the same number of peaks and each peak is within a small angular tolerance of those in the gold standard. The CF is then the fraction of voxels that are consistent with the 96-direction dataset. For voxels that contain multiple fiber populations, the crossing angle is defined as the angle between the two peaks. Finally, the ACC, a measure that describes agreement between spherical functions, is calculated for all voxels in each subsampled dataset.

3. RESULTS

Figure 1 shows Q-ball glyphs in an area containing both single and crossing fiber voxels. Qualitatively, the glyphs seem to share the same basic shape and orientations across all b-values and for all diffusion-weighting schemes. Many glyphs appear more sharp or “spiky” at higher b-values, while very little change is noticeable with changing number of gradient directions.

The average percent deviation from the gold-standard datasets for FA and GFA are shown in Figure 2 (A, B). The percent deviation of FA (Fig 2. A) is monotonically decreasing, and is less than 10% for all b-values after 30 directions. The higher b-values show a consistently higher positive bias than low b-value acquisitions. Unlike FA, the GFA (Fig 2. B) shows very high positive biases at transitions zones that occur when the data first allows the next higher order SH coefficients to be estimated. However, bias decreases as the number of DWIs increases.

Next, the effect of gradient directions on the bias and accuracy of DFF and TH were assessed (Fig 2. C, D). At low DW directions, the DFF is overestimated at all b-values. This is likely due to the inability to resolve multiple fibers, resulting in a DFF of 1 for most voxels. However, at SH of order 6 and 8, the DFF is consistently underestimated, and shows high deviations at the transition zones. Similarly, the deviation of the TH peaks is high at the 28 and 48 direction sets. As the number of DWI’s increases, the peaks sharpness gradually decreases towards the gold-standard TH.

Figure 3 summarizes the reproducibility and accuracy of Q-ball for detecting the presence of multiple fiber populations. The 96-direction data sets suggest that between 60–80% of white matter voxels contain multiple fibers (Fig. 2, A). However, with the exception of 20 and 24 DW-directions, a lower number of directions results in a higher estimate of the prevalence of crossing fibers, with peaks of this measure at SH transition zones. In all cases, a higher b-value results in a larger crossing fiber fraction. The consistency fraction (Fig 2. B) shows that the accuracy of detecting crossing fibers increases with increasing data. However, the consistency is surprisingly low for most datasets, and only reaches 50% at 68 DW-directions. The reason for the low consistency is shown in Figure 2, C. For this figure, we tracked single-fiber, 2-fiber, and 3-fiber datasets (from the gold standard) and calculated the average number of fibers in these voxels in the lower diffusion-direction datasets. It is clear that single fiber voxels consistently (and likely erroneously) resulted in multiple fibers with less DWIs. Similarly, many 2-fiber voxels were estimated to contain 3 fiber populations. Spikes in both functions are seen at SH transition zones. Finally, subtracting the expected crossing angle (from the 96 direction datasets) from the observed crossing angle (from the lower-sampled datasets) for all voxels, we find that there is significant bias when estimating the crossing angle (Fig 2. D). Fibers crossing at angles less than 70° are consistently estimated to be crossing at more orthogonal angles (positive bias), while those with angles between 80° and 90° result in more acute angles when decreasing the number of diffusion weighted directions.

An analysis of the ACC shows that nearly all directions (besides N=28 and N=48) have similar Q-ball SH representations as that of the N=96 dataset, with the average ACC typically 0.8 or higher across the entire brain (Fig 4, A). Qualitatively, the WM dODF profiles agree very well with the gold standard, even at very low gradient directions (Fig 4. B). Low ACC's first become aparrent in gray matter regions, followed by WM in datasets with as many as 56 sampling directions.

4. DISCUSSION

In this study, the aim was to determine the appropriate number of DW-directions for robust estimates of measures derived from Q-ball imaging. What is clear from the data is that the variance and precision of many parameters is dependent on not only the number of directions sampled, but also on the reconstruction scheme, specifically the SH order that the data was fit to. Tournier et al. determine that 8^{th} order SH are high enough to capture the angular profile of the DW signal, which implies that as low as 45 sampling directions is sufficient for all HARDI analysis, although the authors recommend acquisition of more to increase the effective SNR {Tournier, 2013 #1}. Here, we find that fitting 8^{th} order spherical harmonics to just 45 coefficients (or to 28 for SH order 6) leads to noisy and inaccurate estimates of a variety of measures.

Due to fitting the data exactly, the dODFs are noisy at these measurements, overestimate the number of fiber populations in each voxel (Fig. 3, A), and have erroneous peaks (Fig. 3, B and C). This results in temporary increases in GFA (Fig. 2, B), decreases in the DFF (Fig. 2, C), and increase in peak sharpness (Fig. 2, D). Based on these results, we suggest collecting significantly more than the minimum 45 measurements to fit to 8^{th} order SH. It remains to be seen how a 6^{th} order fit to the larger datasets (N>45) compares to the 8^{th} order, and if the accuracy is of a comparable scale. In addition, it is of interest to determine how many directions need to be sampled for the 8^{th} order fit to become more accurate than the same data fit to 6^{th} order. This would answer the question: "given a certain number of sampling directions, and with the aim to estimate parameter X, what order SH is most appropriate to fit my data to?". From our data, for estimates of GFA, DFF, and TH, one must sample approximately 64, 80, and 84 directions for the 8^{th} order fit to be more accurate (lower percent variation) than just 44 directions with 6^{th} order fit. For the ACC, a measure of overall agreement of the dODF, one must sample at least 60 directions to make the jump from 6^{th} to 8^{th} order SH fitting.

Similar recommendations are given when it comes to resolving complex fibers and detecting the number of fiber populations in a voxel. As expected, a higher b-value results in the detection of more crossing fibers in the brain (Fig. 3, A). However, it is interesting that the fraction of fibers containing crossing fibers did not plateau. Thus it is possible that 96 directions are not enough to correctly identify all fiber crossings. It is typically assumed that a higher sampling resolution (more gradient directions) will increase the ability to detect crossing fibers, however, in our data this results in a decreased crossing fiber fraction. The results from our gold-standard data suggest that between 60 and 80% of all white matter voxels contain crossing fibers, a fraction lower than that estimated using alternative HARDI modeling techniques {Jeurissen, 2013 #330}.

The low consistency fraction for all datasets is alarming, particularly with respect to the implications for down-stream fiber tractography. The number of peaks and peak orientations were only consistent with the gold-standard datasets in approximately 80% of white matter voxels using the 92-direction datasets, and only consistent with 50% of these voxels with as many as 68 DW directions (Fig. 3, B). Using capillary phantoms, Cho et al. {Cho, 2008 #820} found that q-ball at a b-value of 3,000 s/mm^2 is able to successfully resolve fibers crossing at 45° in 27% of all voxels, but the success rate increases to 100% at b-values of 4,000 s/mm^2 and above, so it is possible that increasing the diffusion weighting may be able to overcome the low consistency fraction seen in our results. Similarly, simulations {Alexander, 2005 #197} using mixtures of Gaussian test functions suggest that q-ball imaging at clinically relevant SNR resolves two-fiber crossings consistently only if the separate angle is above 85°. While our study did not address the consistency fraction as a function of crossing angle, we did find a bias in the observed crossing angle as the number of diffusion-encoding directions decreased. Literature suggests that Q-ball imaging will *under*-estimate the true crossing angle at low diffusion-weightings {Cho, 2008 #820;Tuch, 2004 #146}. When two fiber populations exist within the same imaging voxel, the dODF can be thought of as having contributions from the dODF from each fiber population separately. However, because a single fiber population has dODF amplitude not only parallel to the fiber directions, but also perpendicular, the addition of these two bundles will create a blurring of the overall dODF, and the two peaks will be shifted towards one another {Anderson, 2009 #821}. However, in our data, we find both over and underestimation of the crossing angle, a bias that depends on the true crossing angle as identified in the 96-direciton datasets. Inter-fiber angles above 80° are consistently underestimated by 5–10°, an effect likely due to the asymmetric distribution of crossing angles (i.e. crossings above 90° are evaluated as 180° minus the crossing angle, due to pi-periodicity). In contrast to literature, inter-fiber angles below 70° are consistently overestimated by 5–10° in our data.

This data set provides the ability to answer several unique questions. First, given a certain amount of time for a HARDI study, which diffusion gradient scheme should be used for optimally accurate HARDI contrasts? This represents a choice between sampling independent directions versus repeated directions: for a fixed number of measurements, is it better to acquire data with the highest angular resolution possible (all gradient directions different), or to acquire less gradient directions, but more averages? Second, this dataset allows us to determine both intra-session and inter-session reproducibility. This would address whether intra-session (physiological noise, distortion artifacts) and inter-session (registration errors) factors dominate the accuracy of HARDI experiments, making the choice of gradient-direction non-significant. Similar analysis has been performed in DTI {Landman, 2007 #75}, but remains largely unanswered for HARDI models.

5. CONCLUSION

In this study, we analyzed the effect of b-value and number of diffusion gradient directions on the accuracy and reproducibility of metrics derived from Q-ball imaging. Our focus was on the ability of Q-ball to extract a discrete number of fiber orientation estimates, as well as information regarding the features of the dODF that can reveal tissue architecture information. We find that measures are highly dependent on the number of directions and the

SH order the data is fit to. Future studies will determine the appropriate SH fit given a specific number of acquired diffusion directions at a given signal-to-noise-ratio. In addition, this unique dataset can be used to determine the optimal acquisition scheme as it related to these metrics. Finally, similar analysis should be performed on a range of HARDI models, to not only optimize acquisitions based on clinical or research needs, but also to determine the limitations of varying HARDI models and suggest future refinements.

Acknowledgments

This work was supported by the National Institutes of Health under award numbers R01EB017230 (Landman) and R01NS058639 (Anderson). This work was conducted in part using the resources of the Advanced Computing Center for Research and Education at Vanderbilt University, Nashville, TN. This project was supported in part by the National Center for Research Resources, Grant UL1 RR024975-01, and is now at the National Center for Advancing Translational Sciences, Grant 2 UL1 TR000445-06. The content is solely the responsibility of the authors and does not necessarily represent the official views of the NIH.

REFERENCES

1. Basser PJ, Mattiello J, LeBihan D. Estimation of the effective self-diffusion tensor from the NMR spin echo. Journal of Magnetic Resonance, Series B. 1994; 103(3):247–254. [PubMed: 8019776]
2. Mori S, van Zijl P. Fiber tracking: principles and strategies–a technical review. NMR in Biomedicine. 2002; 15(7–8):468–480. [PubMed: 12489096]
3. Jeurissen B, Leemans A, Tournier JD, et al. Investigating the prevalence of complex fiber configurations in white matter tissue with diffusion magnetic resonance imaging. Hum Brain Mapp. 2013; 34(11):2747–2766. [PubMed: 22611035]
4. Landman BA, Farrell JA, Jones CK, et al. Effects of diffusion weighting schemes on the reproducibility of DTI-derived fractional anisotropy, mean diffusivity, and principal eigenvector measurements at 1.5T. Neuroimage. 2007; 36(4):1123–1138. [PubMed: 17532649]
5. Jansons KM, Alexander DC. Persistent angular structure: new insights from diffusion magnetic resonance imaging data. Inverse problems. 2003; 19(5):1031.
6. Tournier J, Calamante F, Connelly A. Determination of the appropriate b value and number of gradient directions for high-angular-resolution diffusion-weighted imaging. NMR in Biomedicine. 2013; 26(12):1775–1786. [PubMed: 24038308]
7. Tuch DS. Q-ball imaging. Magnetic resonance in medicine. 2004; 52(6):1358–1372. [PubMed: 15562495]
8. Andersson JL, Skare S, Ashburner J. How to correct susceptibility distortions in spin-echo echo-planar images: application to diffusion tensor imaging. Neuroimage. 2003; 20(2):870–888. [PubMed: 14568458]
9. Andersson JL, Sotiropoulos SN. An integrated approach to correction for off-resonance effects and subject movement in diffusion MR imaging. Neuroimage. 2016; 125:1063–1078. [PubMed: 26481672]
10. Cook P, Bai Y, Nedjati-Gilani S, et al. Camino: open-source diffusion-MRI reconstruction and processing. :2759.
11. Cho KH, Yeh CH, Tournier JD, et al. Evaluation of the accuracy and angular resolution of q-ball imaging. Neuroimage. 2008; 42(1):262–271. [PubMed: 18502152]
12. Alexander DC. Multiple-Fiber Reconstruction Algorithms for Diffusion MRI. Annals of the New York Academy of Sciences. 2005; 1064(1):113–133. [PubMed: 16394152]
13. Tuch DS. Q-ball imaging. Magn Reson Med. 2004; 52(6):1358–1372. [PubMed: 15562495]
14. Anderson AW. How to Do It In Practice - Optimal Approaches to Resolving Fiber Crossings.

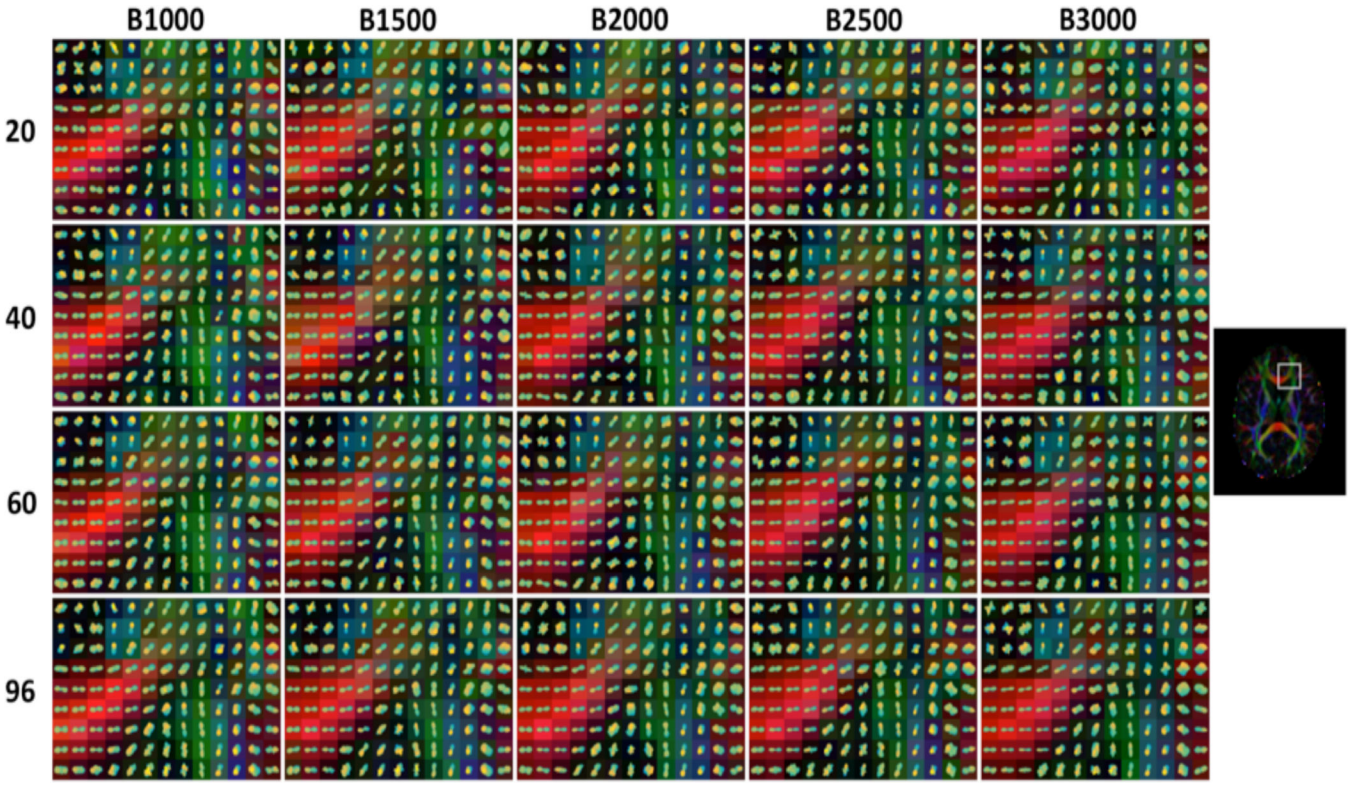

Figure 1.
Qball dODF glyphs for selected datasets, across a range of diffusion-weighted directions and all acquired b-values.

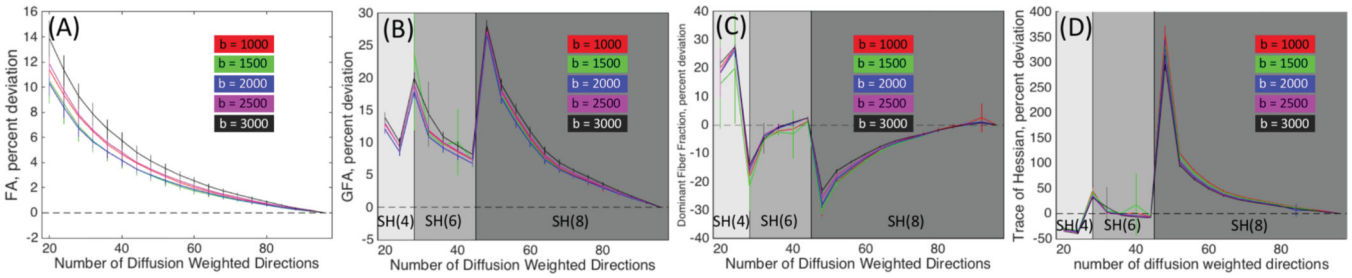

Figure 2.

Percent variation of FA (A), GFA (B), DFF(C), and TH (D) are shown with respect to gold standard dataset, as a function of number of DW directions. Mean and standard deviation across all sessions are displayed for each b-value. Plot backgrounds are colored according to the SH order data was fit to.

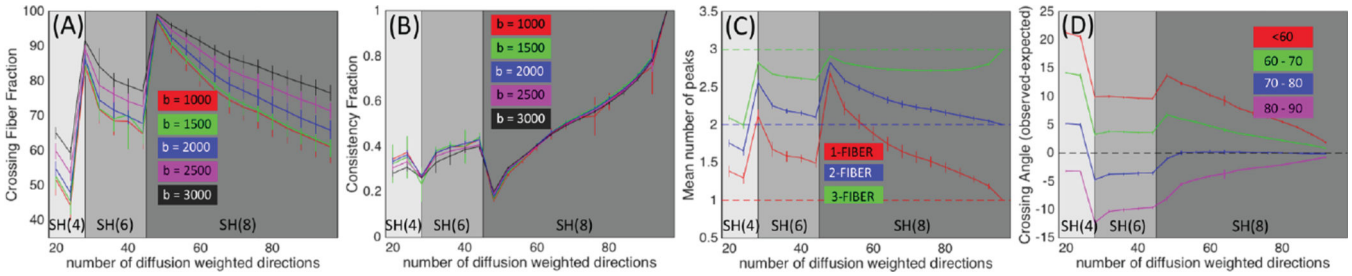

Figure 3.

Crossing fiber analysis. Crossing fiber fraction (A) and Consistency Fraction (B) are shown as a function of number of DW-directions. Mean and standard deviation across all sessions are shown for each b-value. The average number of peaks identified in individual datasets are shown for voxels identified in the gold standard data as having single, 2-fiber, and 3-fiber populations (C) is plotted as a function of number of DW-directions. Angular correlation coefficient between subsampled scan and the gold-standard datasets displayed as images in (H). Finally, the angular bias (observed crossing angle – expected crossing angle) is shown for expected crossing angles of <60, 60–70, 70–80, and 80–90 degrees.

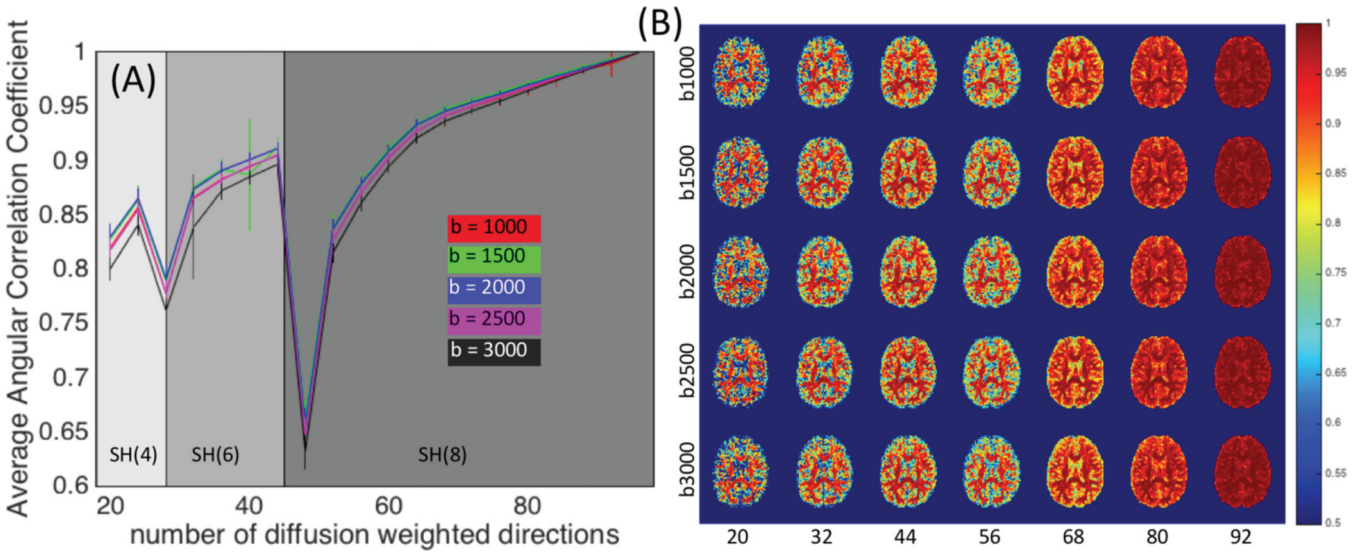

Figure 4.

Angular correlation coefficient between subsampled scan and the gold-standard datasets are plotted for each b-value as a function of number of diffusion weighted directions (A). ACC results are shown for a single subject for selected sets of gradient directions and displayed as images in (B).